ADVANCES IN ATMOSPHERIC SCIENCES, VOL. 33, JULY 2016, 808–818

CMIP5 Simulated Change in the Intensity of the Hadley and Walker Circulations from the Perspective of Velocity Potential

Botao ZHOU*[1,2], Ying SHI[1], and Ying XU[1]

[1]*National Climate Center, China Meteorological Administration, Beijing* 100081

[2]*Collaborative Innovation Center on Forecast and Evaluation of Meteorological Disasters, Nanjing University of Information Science & Technology, Nanjing* 210044

(Received 30 September 2015; revised 21 February 2016; accepted 24 February 2016)

ABSTRACT

Based on the simulations of 31 global models in CMIP5, the performance of the models in simulating the Hadley and Walker circulations is evaluated. In addition, their change in intensity by the end of the 21st century (2080–2099) under the RCP4.5 and RCP8.5 scenarios, relative to 1986–2005, is analyzed from the perspective of 200 hPa velocity potential. Validation shows good performance of the individual CMIP5 models and the multi-model ensemble mean (MME) in reproducing the meridional (zonal) structure and magnitude of Hadley (Walker) circulation. The MME can also capture the observed strengthening tendency of the winter Hadley circulation and weakening tendency of the Walker circulation. Such secular trends can be simulated by 39% and 74% of the models, respectively. The MME projection indicates that the winter Hadley circulation and the Walker circulation will weaken under both scenarios by the end of the 21st century. The weakening amplitude is larger under RCP8.5 than RCP4.5, due to stronger external forcing. The majority of the CMIP5 models show the same projection as the MME. However, for the summer Hadley circulation, the MME shows little change under RCP4.5 and large intermodel spread is apparent. Around half of the models project an increase, and the other half project a decrease. Under the RCP8.5 scenario, the MME and 65% of the models project a weakening of the summer southern Hadley circulation.

Key words: Hadley circulation, Walker circulation, model evaluation, CMIP5 projection, velocity potential

Citation: Zhou, B. T., Y. Shi, and Y. Xu, 2016: CMIP5 Simulated change in the intensity of the Hadley and Walker circulations from the perspective of velocity potential. *Adv. Atmos. Sci.*, **33**(7), 808–818, doi: 10.1007/s00376-016-5216-x.

1. Introduction

The Hadley and Walker circulations are important atmospheric circulations in the tropics. Traditionally, the Hadley circulation refers to a global mean meridional circulation (Held and Hou, 1980; Oort and Yienger, 1996), consisting of overall rising motion near the equator and sinking motion in the subtropics, with the completion of this circuit produced by equatorward motion in the lower troposphere and poleward motion in the upper troposphere. The Walker circulation is a zonal overturning atmospheric circulation, with rising air in the western Pacific and sinking air in the eastern Pacific (Bjerknes, 1969). Their definitions are documented in the glossary of IPCC AR5 (2013). In effect, the Walker circulation can be observed throughout the entire tropical belt. The Hadley and Walker circulations are directly thermally driven and exert significant impacts on climate; for example, they influence temperature and precipitation over a broad range of regions across the globe (Horel and Wallace, 1981; Kousky et al., 1984; Ropelewiski and Halpert, 1989; Hou, 1998; Kumar et al., 2004; Zhou and Wang, 2006a, 2008), and tropical cyclone frequency over the western North Pacific (Zhou and Cui, 2008). They are also closely related to ENSO (Horel and Wallace, 1981; Oort and Yienger, 1996; Wang, 2002a; Quan et al., 2004; Zhou and Wang, 2006b), as summarized in IPCC AR5 (2013). Therefore, the likely change of the Hadley and Walker circulations in a warmer world is a major topic of interest in the climate change research community, as well as those working in other fields of the physical sciences.

The observed secular changes of the Hadley and Walker circulations have been well documented. Several lines of evidence, including reanalyses, layer-average satellite temperatures, and outgoing longwave radiation, indicate that the Hadley circulation in each hemisphere has moved poleward since 1979. The poleward expansion for both hemispheres mainly occurs in their summer and autumn seasons, while changes in their winter and spring seasons are relatively small (Hu and Fu, 2007; Fu and Lin, 2011; Hu et al., 2011; Davis and Rosenlof, 2012; Lucas et al., 2012; Nguyen et al., 2013). Attribution studies suggest that stratospheric ozone depletion

* Corresponding author: Botao ZHOU
Email: zhoubt@cma.gov.cn

and greenhouse gases have made a combined contribution to the poleward expansion of the southern Hadley circulation (SHC) during austral summer (Johanson and Fu, 2009; Polvani et al., 2011; Hu et al., 2013; Min and Son, 2013). Antarctic ozone depletion can cause high-latitude cooling that extends to the troposphere and leads to enhanced meridional temperature gradients between the tropospheric polar region and the extratropics, consequently resulting in a poleward shift of westerly winds and the SHC (Polvani et al., 2011). Greenhouse-gas-induced warming can cause an increase in static stability, such that the onset of baroclinicity is shifted poleward, leading to a poleward expansion of the SHC (Hu and Fu, 2007, Lu et al., 2007). The expansion of the northern Hadley circulation (NHC) during boreal summer has been largely attributed to the increase in black carbon and tropospheric ozone (Allen and Sherwood, 2011). Both of these substances can absorb solar radiation, which warms the extratropical troposphere and causes poleward shifts in the tropospheric subtropical jet stream and the NHC.

It has also been revealed by several studies that the NHC during boreal winter has strengthened, while the SHC during boreal summer has exhibited apparent interdecadal change since the second half of the 20th century (Quan et al., 2004; Zhou and Wang, 2006b). Quan et al. (2004) indicated that the intensification of the NHC during boreal winter may be associated with an intensified hydrological cycle consisting of increased equatorial oceanic rainfall, and a general drying of tropical/subtropical landmasses. Feng et al. (2011) proposed that the interdecadal variation of the SHC may be explained by the non-uniform warming trend in the Indo–western Pacific Ocean and Atlantic Ocean, which increases the large-scale meridional SST gradient in the SH over the Indian Ocean and the tropical Atlantic. However, the mechanism responsible for different behaviors of the NHC and SHC is still an open issue. For the Walker circulation, based on observations of cloud cover, surface wind, vertical velocity and SLP, a weakening tendency is apparent during the 20th century (Vecchi et al., 2006; Nicholls, 2008; Deser et al., 2010; Yu and Zwiers, 2010; Tokinaga et al., 2012). In addition, a number of studies have projected the changes of the Hadley circulation (Frierson et al., 2007; Lu et al., 2007; Hu et al., 2013) and the Walker circulation (Power and Kociuba, 2011; Kociuba and Power, 2015) under future warming.

In the studies mentioned above, the projected changes of the Hadley and Walker circulations were mainly measured by the mass streamfunction and SLP, respectively. Significantly, Wang (2002a, 2002b) used the velocity potential as a characteristic of the Hadley and Walker circulations. Tanaka et al. (2004) further proposed that the Hadley and Walker circulations can be decomposited from the velocity potential in the upper troposphere. In this study, with the aim to provide further clues in the quest to understand changes in the Hadley and Walker circulations, we evaluate the performance of CMIP5 models in simulating the Hadley and Walker circulations and revisit their change from the perspective of velocity potential.

2. Data and method

The simulation data used in this study come from the 31 CMIP5 models listed in Table 1. For each model, the outputs of their historical, RCP4.5 and RCP8.5 experiments (Taylor et al., 2012) are exploited for analysis. The RCP4.5 and RCP8.5 experiments involve the radiative forcing peaking at 4.5 W m^{-2} and 8.5 W m^{-2} by 2100, representing a medium-low and high radiative forcing scenario, respectively. More information on the models and forcings is available on the CMIP5 website (http://cmippcmdi.llnl.gov/cmip5/availability.html). The monthly reanalysis data from NCEP–NCAR (Kistler et al., 2001) during the period 1950–2005 are employed to validate the performance of the CMIP5 models. Since the models have different spatial resolutions (see Table 1), we interpolated them into the same $2.5^\circ \times 2.5^\circ$ grid as the NCEP–NCAR data before analysis.

The velocity potential χ is calculated using the horizontal wind vector $\boldsymbol{V}$ at the 200 hPa level, following the definition by Krishnamurti (1971): $\nabla \cdot \boldsymbol{V} = -\nabla^2\chi$. According to Tanaka et al. (2004), the velocity potential can be divided into the linear combinations of three independent components in terms of its characteristics in the space–time domain, i.e., $\chi(t,x,y) = [\chi](t,y) + \chi^*(t,x,y) = [\chi](t,y) + \overline{\chi^*}(x,y) + \chi^{*'}(t,x,y)$, where x, y, and t represent longitude, latitude and time; $[(\,)]$ and $(\,)^*$ stand for the zonal mean and the deviation from it; and $\overline{(\,)}$ and $(\,)'$ denote the annual mean and the deviation from it, respectively. As stated by Tanaka et al. (2004), the Hadley circulation is defined as an axisymmetric part of the circulation since it is driven by the meridional difference of global zonal-mean heating. This information is assumed to be contained in the zonal-mean field of the velocity potential, i.e., $[\chi](t,y)$. The information on the Walker and monsoonal circulations is then assumed to be contained in the deviation from the zonal mean, i.e., $\chi^*(t,x,y)$. Subsequently, the monsoonal circulation driven essentially by the land–sea heat contrast is defined as part of the seasonal change in the deviation field. For this reason, the annual mean is subtracted from the deviation field of the zonal mean to measure the monsoonal circulation, i.e., $\chi^{*'}(t,x,y)$. Finally, the Walker circulation driven by the different SST along the equatorial tropics is defined as the remainder, which is the annual mean of the zonal deviation field, i.e., $\overline{\chi^*}(x,y)$. Consequently, the Walker circulation has no seasonal variation, which is the shortcoming of this definition. All seasonal cycles are deposited in the monsoonal circulation. Besides, the three separated orthogonal components characterized by the space–time domain may be too simple to separate the complex tropical circulations. Despite the imperfection of this definition, Tanaka et al. (2004) demonstrated that this simple separation of the tropical circulation into the Hadley, Walker and monsoonal components is feasible and useful. The definition retrieves the essence of the tropical circulations and can be used to study their secular changes. Given that the aim here is to analyze the long-term changes of the Hadley and Walker circulations, this approach was adopted in the present study.

Since the NHC and SHC are dominant in boreal win-

Table 1. Information on the 31 CMIP5 models used in the present analysis.

Model name	Modeling group	Atmospheric resolution (lon × lat)
ACCESS1.0	CSIRO and BoM, Australia	192×145
ACCESS1.3	CSIRO and BoM, Australia	192×145
BCC_CSM1.1	BCC, China Meteorological Administration, China	128×64
BCC_CSM1.1(m)	BCC, China Meteorological Administration, China	320×160
BNU-ESM	Beijing Normal University/China	128×64
CanESM2	CCCma, Canada	128×64
CCSM4	NCAR, United States	288×192
CMCC-CM	CMCC, Italy	480×240
CMCC-CMS	CMCC, Italy	192×96
CNRM-CM5	Centre National de Recherches Météorologiques and Centre Europeen de Recherche et Formation Avancees en Calcul Scientifique, France	256×128
CSIRO Mk3.6.0	Queensland Climate Change Centre of Excellence and CSIRO, Australia	192×96
FGOALS-g2	LASG, IAP, Chinese Academy of Sciences, China	128×60
FIO-ESM	First Institute of Oceanography, China	128×64
GFDL CM3	GFDL, NOAA, United States	144×90
GFDL-ESM2G	GFDL, NOAA, United States	144×90
GFDL-ESM2M	GFDL, NOAA, United States	144×90
GISS-E2-H	GISS, NASA, United States	144×90
GISS-E2-R	GISS, NASA, United States	144×90
HadGEM2-AO	Met Office Hadley Centre, United Kingdom	192×144
HadGEM2-ES	Met Office Hadley Centre, United Kingdom	192×144
INMCM4	Institute for Numerical Mathematics, Russia	180×120
IPSL-CM5A-LR	IPSL, France	96×96
IPSL-CM5A-MR	IPSL, France	144×143
IPSL-CM5B-LR	IPSL, France	96×96
MIROC5	Atmosphere and Ocean Research Institute (University of Tokyo), National Institute for Environmental Studies, and Japan Agency for Marine-Earth Science and Technology, Japan	256×128
MIROC-ESM	Atmosphere and Ocean Research Institute (University of Tokyo), National Institute for Environmental Studies, and Japan Agency for Marine-Earth Science and Technology, Japan	128×64
MIROC-ESM-CHEM	Atmosphere and Ocean Research Institute (University of Tokyo), National Institute for Environmental Studies, and Japan Agency for Marine-Earth Science and Technology, Japan	128×64
MPI-ESM-LR	MPI for Meteorology, Germany	192×96
MRI-CGCM3	Meteorological Research Institute, Japan	320×160
NorESM1-M	Norwegian Climate Centre, Norway	144×96
NorESM1-ME	Norwegian Climate Centre, Norway	144×96

ter (December–January–February) and summer (June–July–August), respectively, we just focus on the characteristics of the NHC in boreal winter and the SHC in boreal summer in the following analysis. Note that the Hadley circulation in this study is the global zonal mean, not the local zonal mean. The Walker circulation refers to the annual Pacific Walker circulation, and has no seasonal variations. This problem is not critical for the investigation of its long-term changes (Tanaka et al., 2004).

3. Validation of the CMIP5 models

3.1. *Climatology*

Figure 1 shows the climatological distribution of the velocity potential at 200 hPa during boreal winter and summer, 1986–2005, derived from NCEP–NCAR reanalysis data and the MME simulation of the historical experiment. The corresponding divergent wind is also displayed. The MME is calculated as the arithmetic average of the 31 models. For the NCEP–NCAR reanalysis data, in boreal winter (Fig. 1a), the positive velocity potential with a maximum value above 100×10^5 m^2 s^{-1} is located over the equatorial western Pacific, and the negative velocity potential with a minimum value below -100×10^5 m^2 s^{-1} is observed over western Africa, implying a pronounced zonal wavenumber-one pattern. Since the divergent winds flow from the positive peak to the minimum, strong upward motion occurs over the western Pacific in the SH and the air flows eastward to the equatorial eastern Pacific and northward to Asia. During boreal summer (Fig. 1c), the zonal wavenumber-one pattern is also prominent in the velocity potential. The positive peak, with a value of 190×10^5 m^2 s^{-1} shifts to the northwest near the Philippines, and the minimum, with a value of -135×10^5

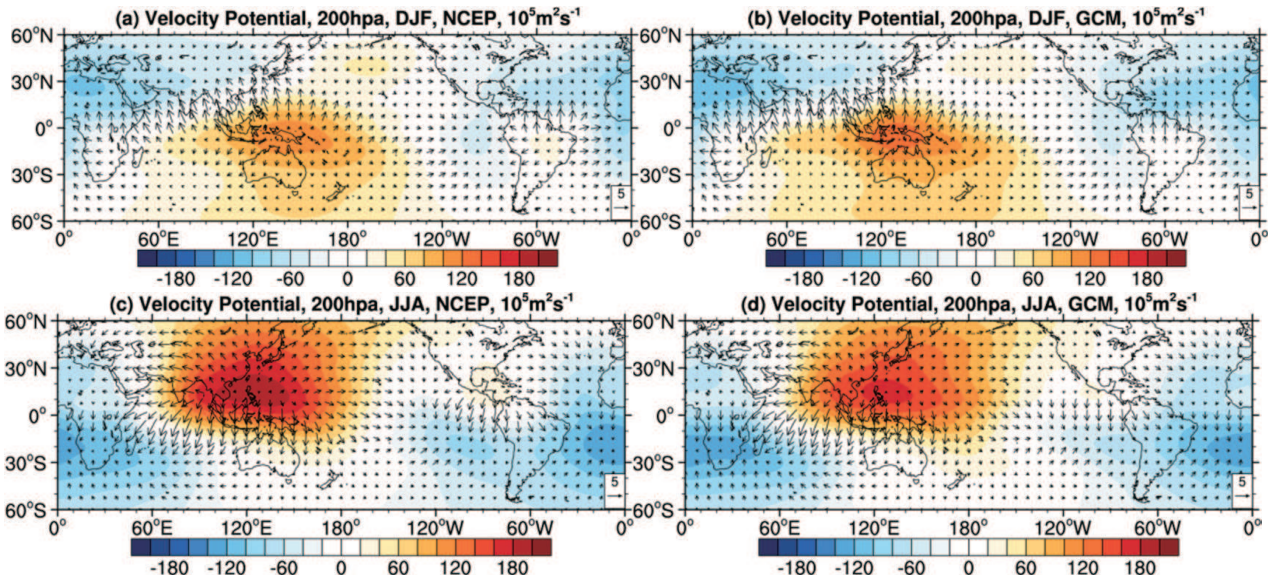

Fig. 1. Climatological distribution of the 200 hPa velocity potential (units: 10^5 m^2 s^{-1}) during boreal (a, b) winter and (c, d) summer of 1986–2005, based on (a, c) NCEP–NCAR reanalysis data and (b, d) the MME simulation.

m^2 s^{-1}, moves southwestward to the South Atlantic. Strong divergent wind is found from the NH to the SH, whose direction over the equator is the reverse of that in boreal winter. This is regarded as the contribution from the Hadley circulation. The velocity potential pattern revealed in the NCEP–NCAR reanalysis data can be reproduced well by the MME. As shown in Figs. 1b and d, the MME simulated patterns in boreal winter and summer are generally comparable to the observation in both spatial distribution and magnitude. The pattern correlation coefficient between the MME simulation and the NCEP–NCAR reanalysis data is 0.96 for boreal winter and 0.98 for boreal summer. The MME can also generally capture the observed spatial structure of the velocity potential in the lower troposphere, which is, however, beyond the scope of the present discussion. For the models on an individual basis, the simulation is also highly correlated to the NCEP–NCAR reanalysis data, with the correlation coefficient ranging from 0.78 (GISS-E2-H) to 0.97 (IPSL-CM5A-LR and IPSL-CM5A-MR), and 0.83 (BCC-CSM1-1-m) to 0.98 (MPI-ESM-LR and CMCC-CMS), for boreal winter and summer, respectively (see Fig. 4).

Figure 2 further presents the zonal mean of the 200 hPa velocity potential in winter and summer for the NCEP–NCAR reanalysis data and the MME simulation. It is interesting to see the general resemblance between them. In boreal winter (Fig. 2a), both exhibit negative values in the NH, with a peak near 25°N, and positive values in the SH, with a peak near 10°S. The negative and positive peaks represent the locations of the sinking branch and rising branch of the NHC, indicating meridional divergent flow from the SH to the NH in the upper troposphere. In boreal summer, the velocity potential at 200 hPa is reversed, being positive in the NH and negative in the SH. The corresponding peaks are respectively located around 15°N and 25°S, and there are upper tropospheric divergent flows from the NH to the SH, indicative of the SHC. The correlation between the NCEP–NCAR reanalysis data and the MME simulation and individual models is higher than 0.90, no matter whether in winter or in summer (see Fig. 4).

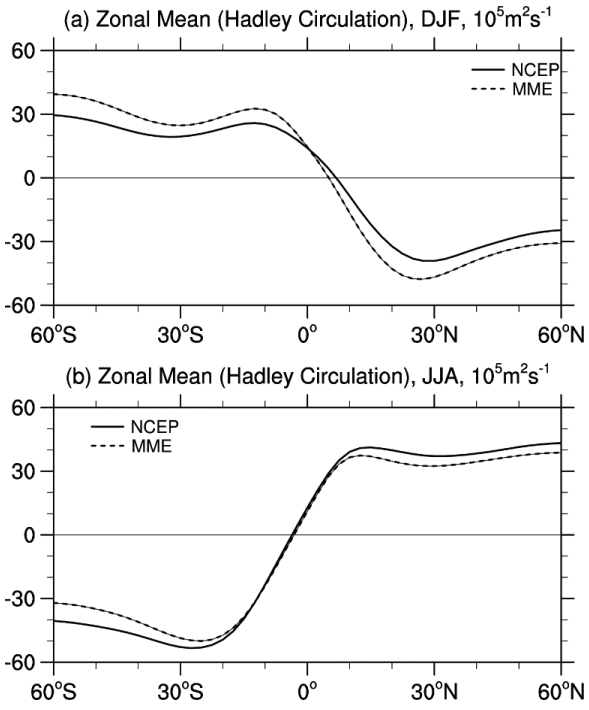

Fig. 2. Zonal mean of the velocity potential (units: 10^5 m^2 s^{-1}) during boreal (a) winter and (b) summer of 1986–2005, based on NCEP–NCAR reanalysis data (solid line) and the MME simulation (dashed line).

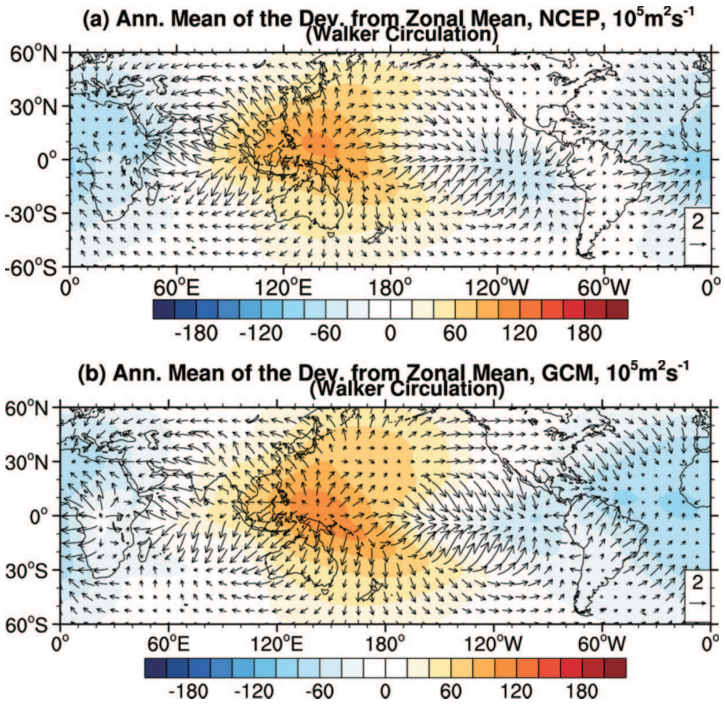

Fig. 3. Annual mean of the deviation from the zonal mean of the velocity potential (units: 10^5 m^2 s^{-1}): (a) NCEP–NCAR reanalysis data; (b) MME simulation.

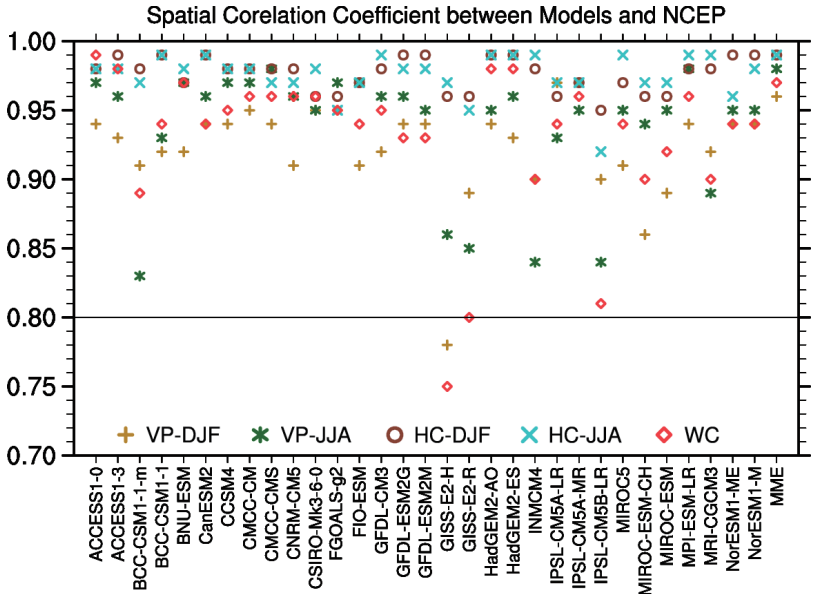

Fig. 4. Spatial correlation coefficient between NCEP–NCAR reanalysis data and the model simulations.

Figures 3a and b display the annual mean deviation from the zonal mean of the velocity potential, superimposed on the divergent winds, for the NCEP–NCAR reanalysis data and the MME simulation, respectively. Comparing these two figures, we can see that they bear a general similarity over the Pacific, with the pattern correlation coefficient being 0.97. Strong and positive velocity potential above 80×10^5 m^2 s^{-1} is dominant over the western Pacific, while strong and negative velocity potential below -40×10^5 m^2 s^{-1} is dominant over the equatorial eastern Pacific. As a consequence, the airflows ascend over the equatorial western Pacific and descend over the eastern Pacific, indicative of the Walker circu-

lation. The correlation coefficients between most of the individual models and the NCEP–NACR reanalysis data are also above 0.90, except models BCC-CSM1-1-m (0.89), GISS-E2-H (0.75), GISS-E2-R (0.80), and IPSL-CM5B-LR (0.81) (see Fig. 4).

3.2. *Trend*

Following Tanaka et al. (2004), we use the peak values of the separated velocity potential to quantify the intensities of the Hadley and Walker circulations. That is, the negative peak value of the zonal-mean velocity potential shown in Figs. 2a and b is defined as the intensity of the winter NHC and the summer SHC, respectively. Certainly, the difference between the positive and negative peaks is another choice for the definition of the intensity. Yet, the restriction such that the global mean is always zero permits us to choose one of the peak values for the alternative simple measure of the intensity. The Walker circulation intensity is defined by the positive peak value of the velocity potential over the western Pacific, as shown in Fig. 3. Tanaka et al. (2004) justified the use of such index definitions to measure the intensity of the Hadley and Walker circulations.

Figure 5 shows the long-term variations of the normalized Hadley and Walker circulation indices for the period 1950–2005 from the NCEP–NCAR reanalysis data. A notable negative trend is apparent in the winter NHC, with a decreasing amplitude of 0.5 $(10\ \mathrm{yr})^{-1}$, significant at the 99% confidence level (Fig. 5a), indicating an intensification of the winter NHC since the 1950s. However, no significant secular trend is detected for the SHC in boreal summer (Fig. 5b). These results conform to those calculated from the mass streamfunction (Quan et al., 2004; Zhou and Wang, 2006b). For the Walker circulation, a significant downward trend exists, with a decreasing amplitude of 0.5 $(10\ \mathrm{yr})^{-1}$, significant at the 99% confidence level, indicating a weakening of the Walker circulation (Fig. 5c).

Trends of the winter NHC, summer SHC and Walker circulation over the same time period in the historical simulations of the MME and individual models are presented in Fig. 6. In general, the sign of secular tendency in the MME simulation complies with the observation, but there is a large spread among individual models. The simulated linear trends range from $-0.20\ (10\ \mathrm{yr})^{-1}$ (CNRM-CM5) to $0.18\ (10\ \mathrm{yr})^{-1}$ (MIROC-ESM-CHEM) for the winter NHC, from $-0.16\ (10\ \mathrm{yr})^{-1}$ (GFDL-ESM2M) to $0.10\ (10\ \mathrm{yr})^{-1}$ (CNRM-CM5) for the summer SHC, and from $-0.20\ (10\ \mathrm{yr})^{-1}$ (IPSL-CM5B-LR) to $0.19\ (10\ \mathrm{yr})^{-1}$ (INMCM4) for the Walker circulation. Among the 31 models, 15 (48%) show positive trends that are in contrast to the observation, and 4 (13%) show small trends for the winter NHC (Fig. 6a). Meanwhile, only 12 (39%) models show negative trends consistent (but underestimated) with the observation. The simulated trends of the Walker circulation are in general better than those for the Hadley circulation. Twenty-three (74%) models can reproduce the negative trends in the observation, in spite of the fact that the observed trend is also underestimated. Only 7 (23%) models show positive trends, and 1 model (3%) shows no change, which differs from the observation (Fig. 6c).

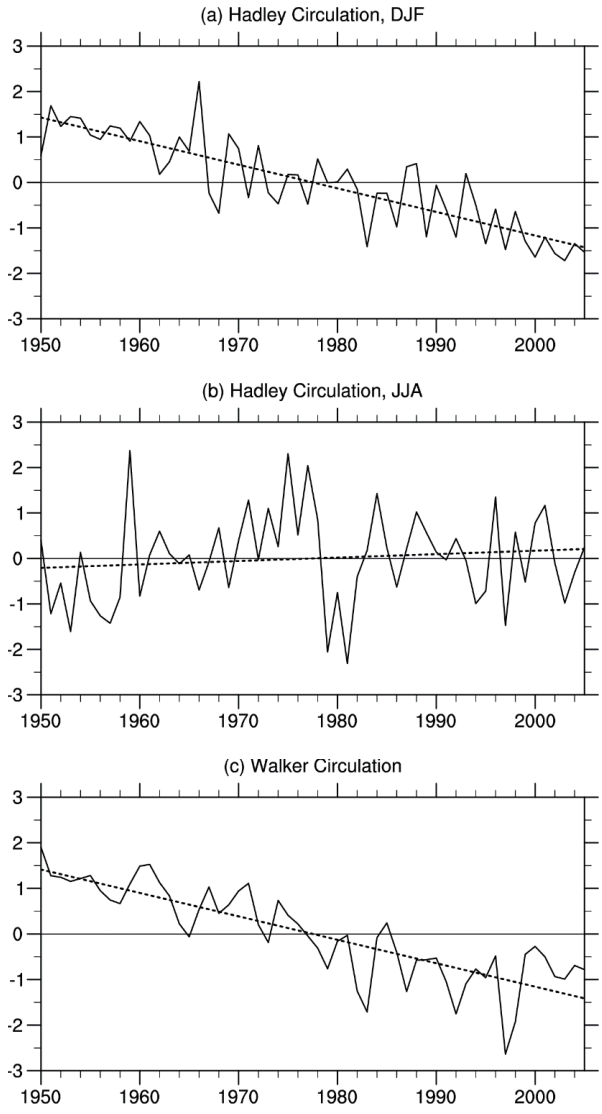

Fig. 5. Temporal change in the normalized intensity index and corresponding trend (dashed line): (a) winter NHC; (b) summer SHC; (c) Walker circulation.

In summary, both the MME and the individual CMIP5 models have good capacity to simulate the observed climatological features of the Hadley and Walker circulations, as defined from the velocity potential in the upper troposphere. The MME as well as 39% and 74% of the models can capture the observed significant trends for the winter NHC and the Walker circulation, respectively, although the observed trend is underestimated.

4. Projected change in the Hadley and Walker circulations

The MME projected temporal evolutions of the intensities of the Hadley and Walker circulations under the RCP4.5 and RCP8.5 scenarios are provided in Fig. 7. An upward trend is clear in the change of the NHC intensity in winter under

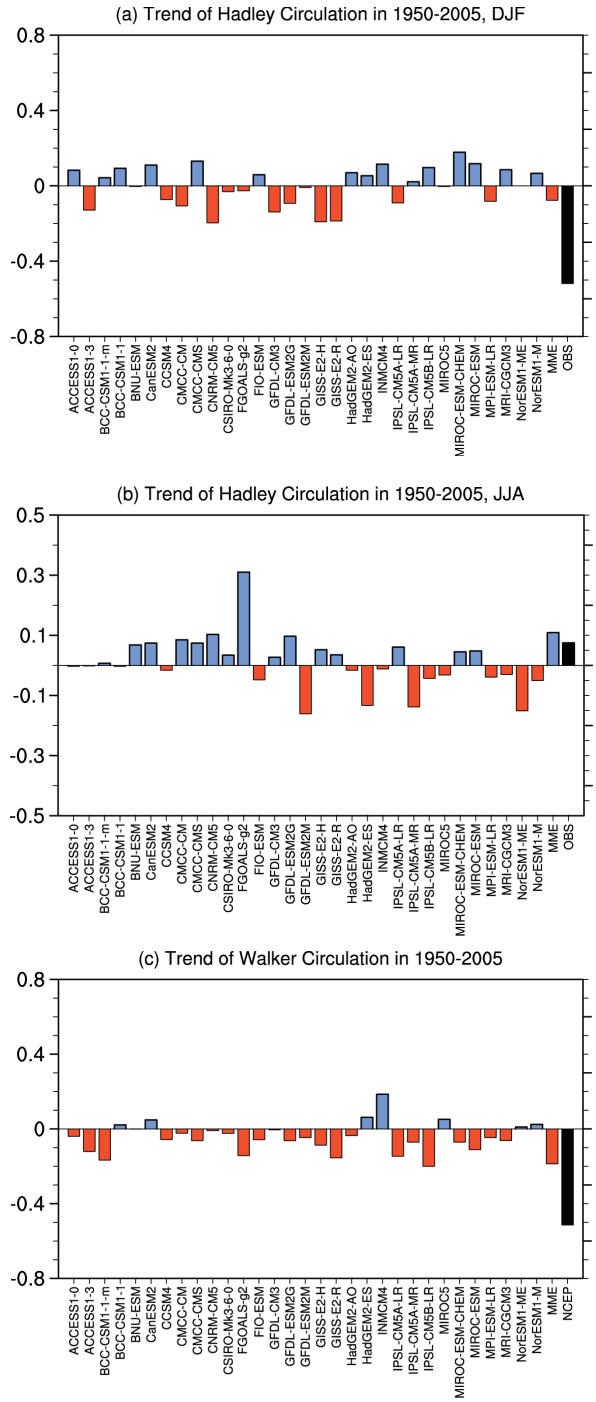

Fig. 6. Trend of the (a) winter NHC, (b) summer SHC and (c) Walker circulation during 1950–2005.

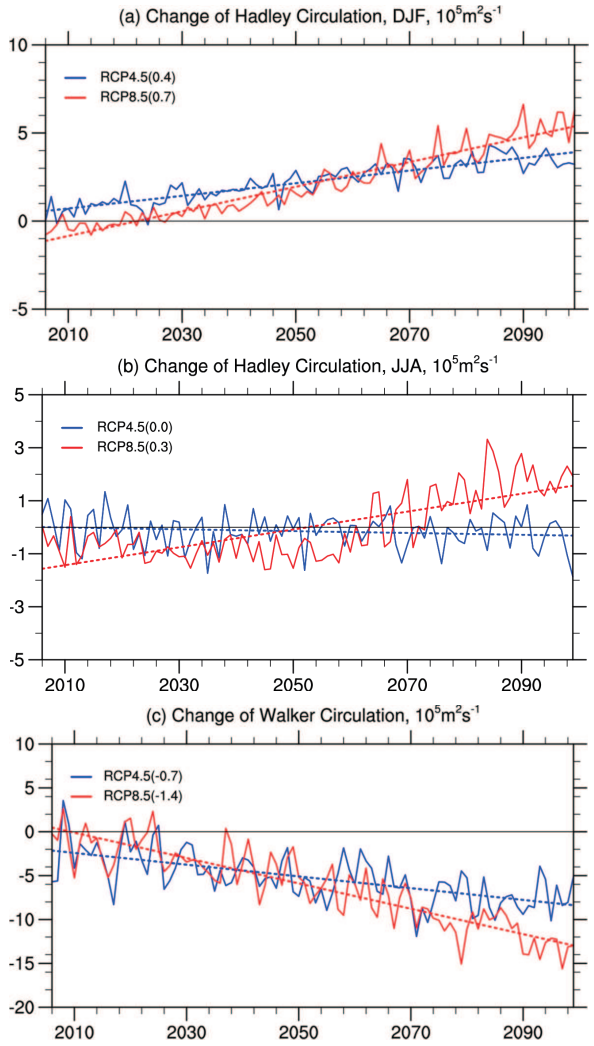

Fig. 7. The MME projected variations and corresponding trends (dashed line) of the intensity index under the RCP4.5 and RCP8.5 scenarios: (a) winter NHC; (b) summer SHC; (c) Walker circulation.

both scenarios, with a larger trend under RCP8.5 [0.7×10^5 m^2 s^{-1} (10 yr)$^{-1}$] than under RCP4.5 [0.4×10^5 m^2 s^{-1} (10 yr)$^{-1}$]. This implies that the winter NHC will weaken toward the end of the 21st century. The intensity of the SHC in boreal summer is also projected to reduce, with a decreasing rate of 0.3×10^5 m^2 s^{-1} (10 yr)$^{-1}$ under the RCP8.5 scenario. However, little change is projected under the RCP4.5 scenario. For the Walker circulation intensity, we find a remarkable decreasing trend under both RCP4.5 and RCP8.5. The rate of decrease is 0.7×10^5 m^2 s^{-1} (10 yr)$^{-1}$ under RCP4.5 and 1.4×10^5 m^2 s^{-1} (10 yr)$^{-1}$ under RCP8.5. Thus, the Walker circulation is also projected to weaken toward the end of the 21st century.

To further explore their future change, we present the spatial distributions of the projected changes in the zonal mean of the velocity potential and the deviation from the zonal mean by the end of the 21st century (2080–99) relative to 1986–2005. As projected in Fig. 8a, the peak of the negative velocity potential—indicating a subsidence of the winter NHC—decreases by 4.4×10^5 m^2 s^{-1} under the RCP4.5 scenario and by 5.3×10^5 m^2 s^{-1} under the RCP8.5 scenario by the end of the 21st century. The SHC intensity in boreal summer is projected to reduce by 2.6×10^5 m^2 s^{-1} under the RCP8.5 scenario (Fig. 8b)—smaller than the change in winter. Under the RCP4.5 scenario, little change is found in the MME projection for the SHC between 2080–99 and 1986–2005. The pro-

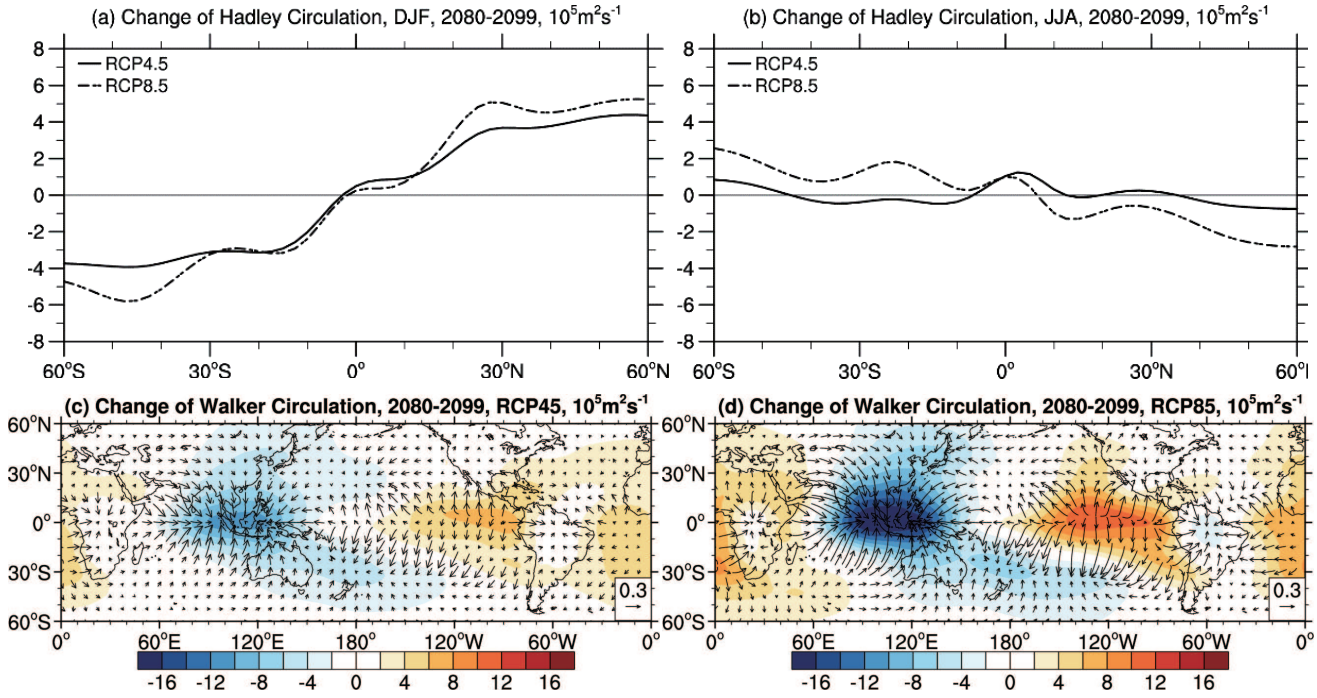

Fig. 8. The MME projected change (units: 10^5 m^2 s^{-1}) of the (a) winter NHC under the RCP4.5 and RCP8.5 scenarios, (b) summer SHC under the RCP4.5 and RCP8.5 scenarios, (c) Walker circulation under the RCP4.5 scenario, and (d) Walker circulation under the RCP8.5 scenario, during 2080–99 (relative to 1986–2005).

jected change in annual mean deviation from the zonal mean of the velocity potential is consistent under the RCP4.5 and RCP8.5 scenarios, with negative anomalies over the equatorial western Pacific and positive anomalies over the equatorial eastern Pacific (Figs. 8c and d). This pattern hints at a weakness in the Walker circulation at the end of the 21st century. The weakening magnitude is much larger under the RCP8.5 scenario than under the RCP4.5 scenario.

To examine the consistency of the projections among individual models, the changes in the intensities of the winter NHC, summer SHC and Walker circulation under the RCP4.5 scenario versus the RCP8.5 scenario are plotted in a scatter diagram (Fig. 9). Apart from GISS-E2-R, INMCM4 and NorESM1-M, all of the models project that the winter NHC intensity will weaken by the end of the 21st century under the two scenarios, with the decreasing amplitude ranging from 0.2×10^5 m^2 s^{-1} to 15.0×10^5 m^2 s^{-1} (Fig. 9a). The inter-model regression equation is $Y = 0.4753X + 0.2824$, suggesting a stronger change in the models under the RCP8.5 scenario than under the RCP4.5 scenario. The MME projects that the intensity will be weakened by 5.6% under RCP4.5 and 10.6% under RCP8.5 at the end of the 21st century, with reference to the period 1986–2005.

For the intensity of the summer SHC, the projected changes are scattered in the range of -4.9×10^5 m^2 s^{-1} to 8.6×10^5 m^2 s^{-1} under the RCP4.5 scenario (ordinate of Fig. 9b) and -5.7×10^5 m^2 s^{-1} to 12.4×10^5 m^2 s^{-1} under the RCP8.5 scenario (abscissa of Fig. 9b). Twenty-nine models are located either in the first quadrant or in the third quadrant, indicating the signs of changes are the same under RCP4.5 and RCP8.5 for most models. The inter-model regression equation is $Y = 0.4703X - 1.601$, also suggesting a stronger change of the models under the RCP8.5 scenario than under the RCP4.5 scenario. Among the 31 CMIP5 models, 13 (42%) models project a decrease in the SHC intensity and 18 (58%) models project an increase, under the RCP4.5 scenario. Thus, the MME projects little change in the SHC intensity under RCP4.5 by the end of the 21st century. For the RCP8.5 scenario, 20 (65%) models project a decrease in the SHC intensity and 11 (35%) models project an increase. As a consequence, the MME projects that the SHC intensity will be weakened by 3.9% at the end of the 21st century, relative to 1986–2005.

For the Walker circulation intensity, the projected changes are scattered in the range of -15.9×10^5 m^2 s^{-1} to 6.2×10^5 m^2 s^{-1} under RCP4.5 (ordinate of Fig. 9c) and -33.1×10^5 m^2 s^{-1} to 12.6×10^5 m^2 s^{-1} under RCP8.5 (abscissa of Fig. 9c). The spread under the RCP8.5 scenario is obviously larger than that under the RCP4.5 scenario, since stronger external forcing is imposed in the models. Among the 31 CMIP5 models, 25 are located either in the first quadrant or in the third quadrant, demonstrating the signs of changes in the Walker circulation intensity are also the same under the RCP4.5 and RCP8.5 scenarios for most models. The inter-model regression equation is $Y = 0.3535X - 1.835$, again revealing a stronger change in the models under the RCP8.5 scenario than under the RCP4.5 scenario. Among the 31 CMIP5 models, 25 (81%) project a decrease in the Walker circulation intensity and 6 (19%) models project an increase, under the RCP4.5 scenario. For the RCP8.5

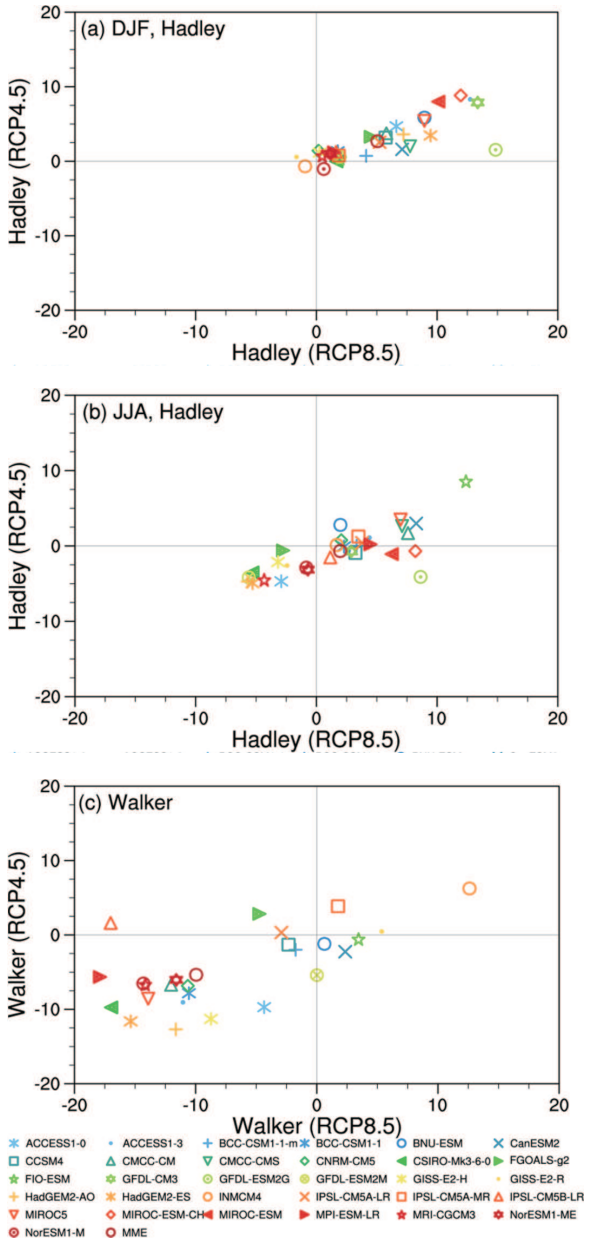

Fig. 9. The RCP4.5 projected changes (ordinate) versus the RCP8.5 projected changes (abscissa) (units: 10^5 m^2 s^{-1}) over 2080–99 relative to 1986–2005: (a) winter NHC; (b) summer SHC; (c) Walker circulation.

scenario, 24 (77%) models project a decrease in the Walker circulation intensity and 7 (23%) project an increase. The MME projects that the intensity will be weakened by 4.9% under RCP4.5 and by 9.2% under RCP8.5, by the end of the 21st century.

5. Conclusion and discussion

Based on the outputs from 31 CMIP5 models, this study evaluates the performance of the models in simulating the features of the Hadley and Walker circulations from the perspective of 200 hPa velocity potential. The results show that the individual CMIP5 models and the MME can successfully capture the climatology of the Hadley circulation in boreal winter and summer, and the Walker circulation. The pattern correlations between the simulations and the observation are generally above 0.9. Besides, the MME can reproduce the strengthening tendency of the winter NHC and the weakening tendency of the Walker circulation in the observation. In terms of individual models, the observed trend in the NHC and the Walker circulation can be simulated (albeit underestimated) by 39% and 74% of them, respectively.

We further project their possible changes under the RCP4.5 and RCP8.5 scenarios. The MME projection indicates that the winter NHC and the Walker circulation are likely to weaken in a warmer world by the end of the 21st century. The weakening tendency under the RCP8.5 scenario is larger than that under the RCP4.5 scenario, since stronger external forcing is imposed in the models. The majority of the CMIP5 models show the same projection as the MME. Nevertheless, for the intensity of the SHC in boreal summer, 42% of the models project a decrease and 58% project an increase, under the RCP4.5 scenario. Thus, its intensity shows little change in the MME projection. Under the RCP8.5 scenario, 65% of models project a decrease and 35% project an increase. As a consequence, its intensity is projected to be weakened by the end of the 21st century, with respect to the period 1986–2005.

Recently, Seo et al. (2014) projected a robust (slight) weakening of the Hadley circulation during boreal winter (summer) at the end of the 21st century under the RCP8.5 scenario, also based on the simulations of CMIP5 models. However, different to our study, they adopted the zonally averaged mass streamfunction to measure the intensity of the Hadley circulation. Nonetheless, the findings are similar, despite the weakening amplitude of the SHC during boreal summer being somewhat different due to the difference in the selected reference period (they used 2001–20, while we used 1986–2005). Similar changes in the Hadley and Walker circulations can also be found in the MME projected vertical–meridional and vertical–zonal planes, respectively (figure not shown).

Changes in the strength of the Hadley circulation are associated with changes in the meridional potential temperature gradient, gross static stability, and tropopause height, and the changes in the meridional potential temperature gradient across the subtropics in a warming climate play a crucial role (Lu et al., 2007; Seo et al., 2014). A reduction in the meridional temperature gradient in response to global warming leads to a reduction in the strength of the Hadley circulation (Seo et al., 2014), which can explain the weakening of the winter NHC and summer SHC. As compared to the RCP4.5 scenario, the greater increase in greenhouse gases under the RCP8.5 scenario induces a greater temperature increase in the subtropics (IPCC, 2013), which results in a larger decrease in the meridional potential temperature gradient and thus a larger reduction in the intensity of the Hadley circulation. The MME projects little change in the

summer SHC strength under the RCP4.5 scenario by the end of the 21st century, which may be linked to the small change in the meridional potential temperature gradient. Changes in the Walker circulation appear to be related to differential warming between the Indian and Pacific Ocean warming at low latitudes (Luo et al., 2012). Over the eastern equatorial Pacific Ocean, where mid-tropospheric ascent is projected to strengthen, changes in zonal SST, and hence SLP gradients, induce low-level westerly wind anomalies that act to weaken the Pacific Walker circulation (IPCC, 2013).

The conclusions drawn in this study reflect a possible estimate by state-of-the-art climate models of the change in tropical circulations. However, due to the uncertainty of the emissions scenarios, uncertainty still exists in projections. Meanwhile, models also possess a number of shortcomings in simulating tropical circulations (Hu et al., 2013; Ma and Zhou, 2014; Kociuba and Power, 2015), possibly imposing further uncertainty upon the conclusions. In addition to the intensity, there are other important aspects of the Hadley and Walker circulations to consider, including spatial localization, inclination, and vertical structure. Moreover, the characteristics and contributions of local meridional circulations in different regions to the global zonal mean Hadley circulation are different and even opposite. How well do CMIP5 models simulate these, and what changes in them can we expect in the future? These issues need to be studied further in future work.

Acknowledgements. We acknowledge the World Climate Research Program's Working Group on Coupled Modeling, which is responsible for CMIP, and thank the climate modeling groups for producing and making available their model output. This research was jointly supported by the National Natural Science Foundation (Grant No. 41275078), the Special Fund for Public Welfare Industry (Meteorology) (Grant No. GYHY201306026) and the National Science & Technology Pillar Program (Grant No. 2012BAC20B05) of China.

REFERENCES

Allen, R. J., and S. C. Sherwood, 2011: The impact of natural versus anthropogenic aerosols on atmospheric circulation in the Community Atmosphere Model. *Climate Dyn.*, **36**, 1959–1978.

Bjerknes, J., 1969: Atmospheric teleconnections from the Equatorial Pacific. *Mon. Wea. Rev.*, **97**, 163–172.

Davis, S. M., and K. H. Rosenlof, 2012: A multidiagnostic intercomparison of tropical-width time series using reanalyses and satellite observations. *J. Climate*, **25**, 1061–1078.

Deser, C., A. S. Phillips, and M. A. Alexander, 2010: Twentieth century tropical sea surface temperature trends revisited. *Geophys. Res. Lett.*, **37**, L10701, doi: 10.1029/2010GL043321.

Feng, R., J. P. Li, and J. C. Wang, 2011: The principal modes of variability of the boreal summer Hadley circulation and their variations. *Chinese Journal of Atmospheric Sciences*, **35**, 201–206. (in Chinese)

Frierson, D. M. W., J. Lu, and G. Chen, 2007: Width of the Hadley cell in simple and comprehensive general circulation models. *Geophys. Res. Lett.*, **34**, L18804, doi: 10.1029/2007GL031115.

Fu, Q., and P. Lin, 2011: Poleward shift of subtropical jets inferred from satellite-observed lower-stratospheric temperatures. *J. Climate*, **24**, 5597–5603.

Held, I. M., and A. Y. Hou, 1980: Nonlinear axially symmetric circulations in a nearly inviscid atmosphere. *J. Atmos. Sci.*, **37**, 515–533.

Horel, J. D., and J. M. Wallace, 1981: Planetary-scale atmospheric phenomena associated with the Southern Oscillation. *Mon. Wea. Rev.*, **109**, 813–829.

Hou, A. Y., 1998: Hadley circulation as a modulator of the extratropical climate. *J. Atmos. Sci.*, **55**, 2437–2457.

Hu, Y., and Q. Fu, 2007: Observed poleward expansion of the Hadley circulation since 1979. *Atmos. Chem. Phys.*, **7**, 5229–5236.

Hu, Y. Y., C. Zhou, and J. P. Liu, 2011: Observational evidence for poleward expansion of the Hadley circulation. *Adv. Atmos. Sci.*, **28**, 33–44, doi: 10.1007/s00376-010-0032-1.

Hu, Y. Y., L. J. Tao, and J. P. Liu, 2013: Poleward expansion of the Hadley circulation in CMIP5 simulations. *Adv. Atmos. Sci.*, **30**, 790–795, doi: 10.1007/s00376-012-2187-4.

IPCC, 2013: Climate Change 2013: The Physical Science Basis. *Contribution of Working Group I to the Fifth Assessment Report of the Intergovernmental Panel on Climate Change.* Cambridge University Press, Cambridge, UK and New York, NY, 1535 pp.

Johanson, C. M., and Q. Fu, 2009: Hadley cell widening: Model simulations versus observations. *J. Climate*, **22**, 2713–2725.

Kistler, R., and Coauthors, 2001: The NCEP-NCAR 50-year reanalysis: Monthly means CD-ROM and documentation. *Bull. Amer. Meteor. Soc.*, **82**, 247–267.

Kociuba, G., and S. B. Power, 2015: Inability of CMIP5 models to simulate recent strengthening of the Walker Circulation: Implications for projections. *J. Climate*, **28**, 20–35.

Kousky, V. E., M. T. Kagano, and I. F. A. Cavalcanti, 1984: A review of the Southern Oscillation: Oceanic-atmospheric circulation changes and related rainfall anomalies. *Tellus A*, **36A**, 490–504.

Kumar, A., F. L. Yang, L. Goddard, and S. Schubert, 2004: Differing trends in the tropical surface temperatures and precipitation over land and oceans. *J. Climate*, **17**, 653–664.

Krishnamurti, T. N., 1971: Tropical east–west circulations during the northern summer. *J. Atmos. Sci.*, **28**, 1342–1347.

Lu, J., G. A. Vecchi, and T. Reichler, 2007: Expansion of the Hadley cell under global warming. *Geophys. Res. Lett.*, **34**, L06805, doi: 10.1029/2006GL028443.

Lucas, C., H. Nguyen, and B. Timbal, 2012: An observational analysis of Southern Hemisphere tropical expansion. *J. Geophys. Res.*, **117**, D17112, doi: 10.1029/2011JD017033.

Luo, J. J., W. Sasaki, and Y. Masumoto, 2012: Indian Ocean warming modulates Pacific climate change. *Proceedings of the National Academy of Sciences of the United States of America*, **109**, 18701–18706.

Ma, S. M., and T. J. Zhou, 2014: Changes of the tropical Pacific Walker circulation simulated by two versions of FGOALS model. *Science China Earth Sciences*, **57**, 2165–2180.

Min, S.-K., and S.-W. Son, 2013: Multimodel attribution of the Southern Hemisphere Hadley cell widening: Major role of ozone depletion. *J. Geophys. Res.: Atmos.*, **118**, 3007–3015, doi: 10.1002/jgrd.50232.

Nguyen, H., A. Evans, C. Lucas, I. Smith, and B. Timbal, 2013: The Hadley circulation in reanalyses: Climatology, variabil-

ity, and change. *J. Climate*, **26**, 3357–3376.

Nicholls, N., 2008: Recent trends in the seasonal and temporal behaviour of the El Niño-Southern Oscillation. *Geophys. Res. Lett.*, **35**, L19703, doi: 10.1029/2008GL034499.

Oort, A. H., and J. J. Yienger, 1996: Observed interannual variability in the Hadley circulation and its connection to ENSO. *J. Climate*, **9**, 2751–2767.

Polvani, L. M., D. W. Waugh, G. J. P. Correa, and S. W. Son, 2011: Stratospheric ozone depletion: The main driver of twentieth-century atmospheric circulation changes in the southern hemisphere. *J. Climate*, **24**, 795–812.

Power, S. B., and G. Kociuba, 2011: The impact of global warming on the Southern Oscillation Index. *Climate Dyn.*, **37**, 1745–1754.

Quan, X. W., H. F. Diaz, and M. P. Hoerling, 2004: Change in the tropical Hadley cell since 1950. *The Hadley Circulation: Past, Present, and Future*, H. F. Diaz and R. S. Bradley, Eds., Springer, 85–120.

Ropelewiski, C. F., and M. S. Halpert, 1989: Precipitation patterns associated with the high index phase of the Southern Oscillation. *J. Climate*, **2**, 268–284.

Seo, K. H., D. M. W. Frierson, and J. H. Son, 2014: A mechanism for future changes in Hadley circulation strength in CMIP5 climate change simulations. *Geophys. Res. Lett.*, **41**, 5251–5258, doi: 10.1002/2014GL060868.

Tanaka, H. L., N. Ishizaki, and A. Kitoh, 2004: Trend and interannual variability of Walker, monsoon and Hadley circulations defined by velocity potential in the upper troposphere. *Tellus A*, **56**, 250–269.

Taylor, K. E., B. J. Stouffer, and G. A. Meehl, 2012: An overview of CMIP5 and the experiment design. *Bull. Amer. Meteor. Soc.*, **93**, 485–498.

Tokinaga, H., S.-P. Xie, C. Deser, Y. Kosaka, and Y. M. Okumura, 2012: Slowdown of the Walker circulation driven by tropical Indo-Pacific warming. *Nature*, **491**, 439–443.

Vecchi, G. A., B. J. Soden, A. T. Wittenberg, I. M. Held, A. Leetmaa, and M. J. Harrison, 2006: Weakening of tropical Pacific atmospheric circulation due to anthropogenic forcing. *Nature*, **441**, 73–76.

Wang, C. Z., 2002a: Atmospheric circulation cells associated with the El Niño-Southern Oscillation. *J. Climate*, **15**, 399–419.

Wang, C. Z., 2002b: Atlantic climate variability and its associated atmospheric circulation cells. *J. Climate*, **15**, 1516–1536.

Yu, B., and F. W. Zwiers, 2010: Changes in equatorial atmospheric zonal circulations in recent decades. *Geophys. Res. Lett.*, **37**, L05701, doi: 10.1029/2009GL042071.

Zhou, B. T., and J. H. Wang, 2006a: Relationship between the boreal spring Hadley circulation and the summer precipitation in the Yangtze River valley. *J. Geophys. Res.*, **111**, D16109, doi: 10.1029/2005JD007006.

Zhou, B. T., and H. J. Wang, 2006b: Interannual and interdecadal variations of the Hadley circulation and its connection with tropical sea surface temperature. *Chinese Journal of Geophysics*, **49**(5), 1147–1154.

Zhou, B. T., and H. J. Wang, 2008: Relationship between Hadley circulation and sea ice extent in the Bering sea. *Chinese Science Bulletin*, **53**(3), 444–449.

Zhou, B. T., and X. Cui, 2008: Hadley circulation signal in the tropical cyclone frequency over the western North Pacific. *J. Geophys. Res.*, **113**, D16107, doi: 10.1029/2007JD009156.